IEEE Access
Multidisciplinary : Rapid Review : Open Access Journal

A Zero-Voltage-Transition H5-Type Transformerless Photovoltaic Grid-Connected Inverter

Jicheng Fang [1], Mingming Shi [2], Huafeng Xiao [3] and Ruibin Wang [3]

[1] School of Electronics and Information Engineering, Shanghai University of Electric Power, Shanghai, 200090 China
[2] State Grid Jiangsu Electric Power Co., LTD. Research Institute, Nanjing, 210000 China
[3] School of Electrical Engineering, Southeast University, Nanjing, 210000 China

Corresponding author: Jicheng Fang (e-mail: fangjicheng_xs@126.com).

ABSTRACT Efficiency and leakage current are two major issues for transformerless grid-connected inverters (TLI). Soft-switching technologies can reduce switching losses and be applied in TLIs. Herein, a zero-voltage-transition H5 type (ZVT-H5) inverter with soft turn-on and turn-off transitions of high-frequency main switches is derived from basic resonant tanks. Compared with the hard-switching H5 (HS-H5) inverter, the conversion efficiency of ZVT-H5 is significantly improved. Moreover, the reverse recovery problem of freewheeling diodes is alleviated under the operation of the auxiliary resonant network. Meanwhile, a diode clamping branch is employed to achieve constant common-mode characteristic for the ZVT-H5. The construction process of the proposed topology is described, and the operation principle of the auxiliary resonant network is analyzed. Moreover, the resonant parameter design of ZVT-H5 and its circuit performance are discussed in detail. Finally, the experimental results of a 3-kW prototype at 100 kHz switching frequency are provided to verify the effectiveness of the ZVT-H5.

INDEX TERMS Grid-connected inverter; Transformerless; Zero-voltage-transition (ZVT); Resonant tank

I. INTRODUCTION

Recently, the distributed photovoltaic generation system has been applied in many areas. Transformerless PV generation configurations have become widely accepted due to their high efficiency, small volume and low cost [1-3]. Several transformerless inverters such as HERIC [4], H5 [5], H6 [6], neutral-point-clamped inverter [7], etc., have been extensively used in PV power systems rated from 2.5 to 8 kW because of their high reliability and simplicity. However, in conventional transformerless PV grid-connected inverters, their switching frequency is still chosen at a lower level for maintaining the converter efficiency, which limits the miniaturization of passive components.

Employing wide bandgap (WBG) devices as power switches can effectively reduce switching losses, which facilitates to increase switching frequency as well as power density for TLIs [8]. However, some challenges, such as severe switching stresses and electromagnetic interference (EMI) caused by the high switching speed of WBGs, should be addressed [9].

Obviously, the soft-switching technique is an alternative way to achieve high conversion efficiency with increased switching frequency. In addition, another advantage of low dv/dt and di/dt stresses can eliminate EMI

noise [10]. Recently, the soft-switching technique for transformerless PV grid-connected inverters has attracted the increasing attention. The auxiliary resonant commutated pole concept, the resonant dc link concept and resonant ac link concept were brought into PV inverters in literature [11], [12] and [13], respectively. These soft-switching technologies are effective to reduce switching losses.

However, the resonant action of the passive components could worsen the PV inverters' differential-mode voltage (DMV) and common-mode voltage (CMV) performance, which closely relates to the implement of high efficiency and low leakage current in TLIs, respectively. For example, Gekeler used a passive snubber circuit to construct a soft-switching three-level inverter in literature [15] and the added passive components can avoid the switching loss in switches and diodes. However, due to the reset of the resonant inductor current, a two-level differential-mode voltage appeared in the commutation period deteriorated the differential-mode characteristic.

In order to realize soft-switching operation and retain good DMV and CMV performance simultaneously, this study focuses on designing a zero-voltage-transition configuration based on the H5 topology because it has realized a tradeoff between the conversion efficiency and

leakage current suppression performance compared with other typical TLI topologies [15]. In addition, both of them can be further improved with the added ZVT resonant network and freewheeling clamping branch, respectively. Meanwhile, the resonance operation of the proposed ZVT-H5 has no negative effect on its differential-mode features.

The paper is structured as follows. Section Ⅱ presents the circuit structure of the improved ZVT-H5 topology. Operation modes of the ZVT-H5 topology are discussed in detail in Section Ⅲ. Section Ⅳ explains the resonant parameter design of ZVT-H5 and analyzes the circuit performance. Experimental results of a 100 kHz, 3 kW ZVT-H5 are discussed in Section Ⅴ. Finally, the conclusion is provided in Section Ⅵ.

II. CIRCUIT STRUCTURE OF THE IMPROVED ZVT-H5

As illustrated in FIGURE 1(a), the HS-H5 topology involves an extra fifth switch S_5 compared with the classical full bridge inverter in order to decouple PV array from the grid during freewheeling period. And the current flows through three switches in the power processing period. The current loop includes S_5, S_1, and S_4 in the positive half cycle, which results in slightly larger conduction losses compared with the HERIC topology (only two switches included in its current loop in the corresponding stages) under unified circuit parameters, as shown in FIGURE 1(b).
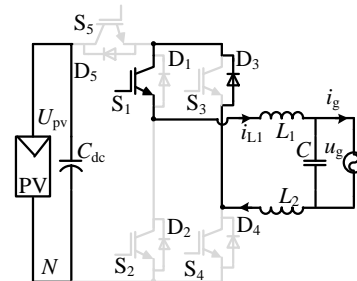
The equivalent circuit of the freewheeling period of H5 is shown in FIGURE 1(c). Due to parasitic parameters, the potential of its freewheeling path may deviate from the midpoint voltage, which results in a high-frequency common-mode voltage and poor leakage current suppression performance.
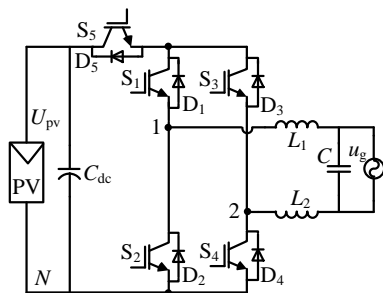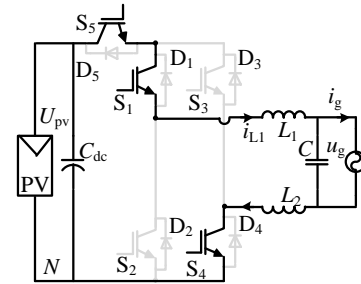
(b) Power transmission mode

(c) Freewheeling mode

FIGURE 1. The circuit structure and working modes of HS-H5

In order to improve the conversion efficiency of H5 and eliminate the high-frequency fluctuation of its common-mode voltage, a novel ZVT resonant network and diode clamping branch are employed in this study. The construction process of ZVT-H5 is shown in FIGURE 2. Specifically, the added resonant network assists in realizing zero-voltage turn-on and turn-off for high-frequency main switches, and zero-current turn-on for high-frequency auxiliary switches, which significantly reduces the switching loss of H5. Meanwhile, the common-mode voltage can be a constant value during the whole switching period with the assistance of the inserted diode clamping branch, as shown in FIGURE 2(c). In ZVT-H5, MOSFETs are chosen as high-frequency switches to use their junction capacitance as part of resonant parameters [16,17].

In FIGURE 2(b), the main switch S_5 has its own resonant tank with a positive DC bus polarity and two main switches S_2 and S_4, which can be activated line-frequency alternately with unipolar sinusoidal pulse width modulation (SPWM), share one integrated resonant tank. Both resonant tanks are in parallel with the power flow of H5 and connect with the DC bus and AC side at the same time. In addition, the freewheeling diode branch is linked between two tanks.
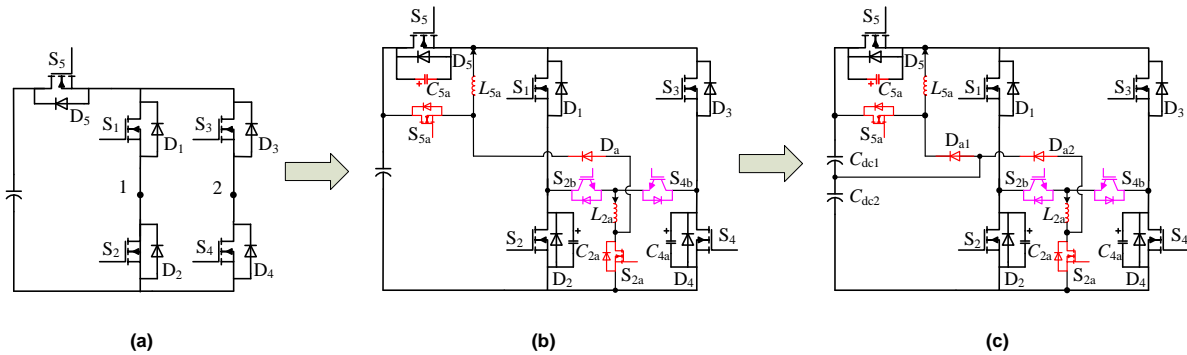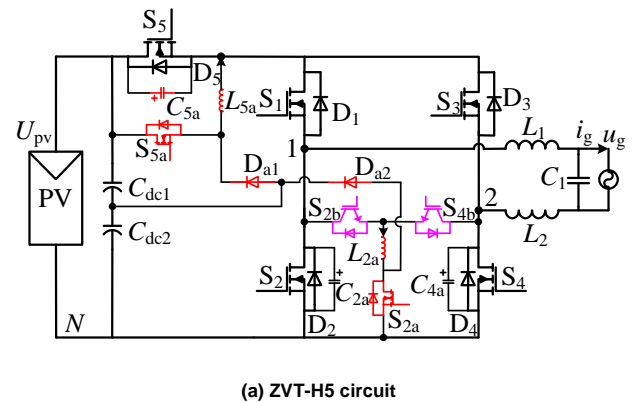

(a) HS-H5 topology

FIGURE 2. The construction process of the ZVT-H5. (a) HS-H5 topology;(b) ZVT-H5 with added resonant tanks;(c) ZVT-H5 with added resonant tanks and clamping diodes.

As shown in FIGURE 2(c), in order to gain the clamping ability of the common-mode voltage in the freewheeling period and decrease the voltage stress of the freewheeling diode D_a (equals to the DC input voltage), both of the voltage-dividing capacitors C_{dc1}/C_{dc2} and diode clamping branch composed by D_{a1} and D_{a2} are included, which replaces the freewheeling diode branch in FIGURE 2(b). As a consequence, the voltage stress of D_{a1} and D_{a2} are reduced to half of the input voltage, contributing to low voltage rated power diodes in this inverter. More importantly, the common-mode voltage can be clamped to half of the input voltage in the freewheeling period, which is important to leakage current indicators [18-20].
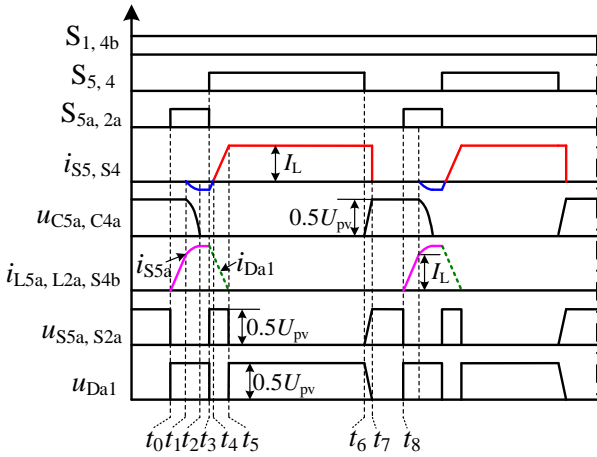
III. OPERATION PRINCIPLE OF ZVT-H5

The derived ZVT-H5 topology with PV power source and the grid-connected filter is illustrated in FIGURE 3(a). The top resonant tank consists of the auxiliary switch S_{5a}, resonant capacitor C_{5a}, and resonant inductor L_{5a}. The bottom resonant tank is composed of the auxiliary switches S_{2a}, S_{2b}, S_{4b} and the resonant components C_{2a}, C_{4a}, L_2. Meanwhile, $L_{5a}=L_{2a}=L_r$ and $C_{5a}=C_{2a}=C_{4a}=C_r$. In this inverter, S_5, S_2, and S_4 are the high frequency main switches; S_1 and S_3 are the line frequency freewheeling switches; D_{a1} and D_{a2} are the freewheeling diodes. L_1, L_2, and C_1 form the filter connected to the grid.

FIGURE 3(b) presents driving signals of the proposed ZVT-H5 topology. It appears that S_5 and S_4 share the same driving signals in the positive half cycle; correspondingly, the driving signals of S_5 and S_2 are the same in negative half cycle. In addition, the same driving signals of S_{5a} and S_{2a} work in the entire grid period. The same driving signals of S_1 and S_{4b} are driven line-frequency complementarily with S_3 and S_{2b}.

(a) ZVT-H5 circuit
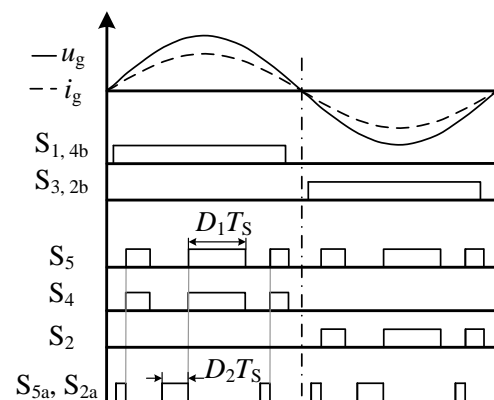
(b) Driving logic in grid frequency scale

(c) Key waveforms in switching frequency scale

FIGURE 3. The **novel ZVT-H5 full bridge transformerless photovoltaic grid-connected inverter**

Several assumptions are made to facilitate the operation principle analysis: 1) All semiconductor devices are ideal switches without parasitic parameters; 2) Due to the large DC capacitance C_{dc1} and C_{dc2}, it can be treated as a constant voltage source. Correspondingly, the filter inductances L_1 and L_2 are also large enough to be treated as a constant current source in every switching period. FIGURE 3(b) shows the driving logic of the ZVT-H5 at the grid frequency scale. It clearly shows that in a positive half cycle of the grid-in current, S_1 and S_{4b} are always ON while S_3 and S_{2b} are always OFF. Reversely, S_1 and S_{4b} are always OFF while S_3 and S_{2b} are always ON in the negative half cycle. Apparently, the majority of the switching losses root in the high-frequency switches S_5, S_2 and S_4 and the switching losses of line-frequency blocking switches are relatively ignorable. One complete switching period can be divided into nine stages. Because of the similarity, only the operation modes in the positive half period of the grid-in current are illustrated in detail.

1) *Stage 1 [t_0, t_1]:* Before t_0, S_1 and S_{4b} are on and S_5, S_2, S_4, S_{5a}, S_{2a}, S_{2b}, and S_3 are off. As shown in FIGURE 4(h), it is in the normal freewheeling period same as the H5 topology. Meanwhile, the resonant capacitors voltage u_{Ca} of C_{5a}, C_{2a} and C_{4a} is a constant value, which is half of the input voltage; the current i_{La} through the resonant inductors L_{5a} and L_{2a} are zero, $i_{L5a}=i_{L2a}=0$; and the current through the filter inductors L_1 and L_2 is I_L. At t_0, S_{5a} and S_{2a} are turned on, and the resonant inductor currents i_{L5a}, and i_{L2a} increase linearly under the effect of the voltage $0.5U_{PV}$ until they reach I_L at t_1, respectively. Therefore, the resonant switches S_{5a} and S_{2a} can be turned on with zero current. The equivalent circuit is shown in FIGURE 4(a). In this stage,

$$i_{La}(t) = \frac{U_{PV}}{2L_r}(t - t_0) \tag{1}$$

Meanwhile, the current through D_3 is linearly decreased from $0.5I_L$ to 0. At t_1, the current through the diode D_3 falls to zero. As a result, the ZCS turn-off condition of the anti-parallel diode of S_3 is achieved, and its reverse recovery problem is then alleviated.
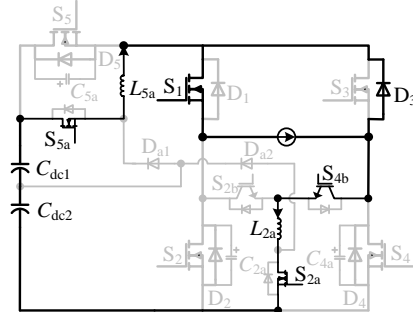
2) *Stage 2 [t_1, t_2]:* According to FIGURE 4(b), the resonant components C_{5a} and L_{5a} together with C_{4a} and L_{2a} construct two resonant tanks and then begin to resonate at t_1, respectively. At t_2, the resonant current i_{La} increases to the peak current (I_L+I_{Ra}) while the resonant voltages u_{Ca} across C_{5a} and C_{4a} begin to reduce until it reaches to zero at t_2. Therefore, the main switches S_5 and S_4 can be turned on with ZVS condition. In this stage,

$$i_{La}(t) = I_L + \frac{U_{PV}}{2Z_r}\sin\omega_r(t - t_1) \tag{2}$$

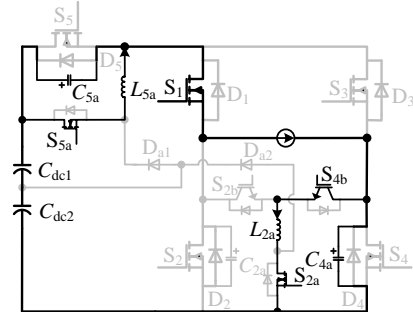$$u_{Ca}(t) = \frac{U_{PV}}{2}\cos\omega_r(t - t_1) \tag{3}$$

$$t_2 - t_1 = \frac{1}{4}T_r \tag{4}$$

where $\omega_r = 1/\sqrt{L_r C_r}$、$Z_r = \sqrt{L_r/C_r}$、$T_r = 2\pi\sqrt{L_r C_r}$、$I_{Ra} = U_{PV}/2Z_r$.

(a)Stage 1 [t_0, t_1]

(b)Stage 2 [t_1, t_2]

(c) Stage 3 [t_2, t_3]

(d) Stage 4 [t_3, t_4]

(e)Stage 5 [t_4, t_5]

(f) Stage 6 [t_5, t_6]

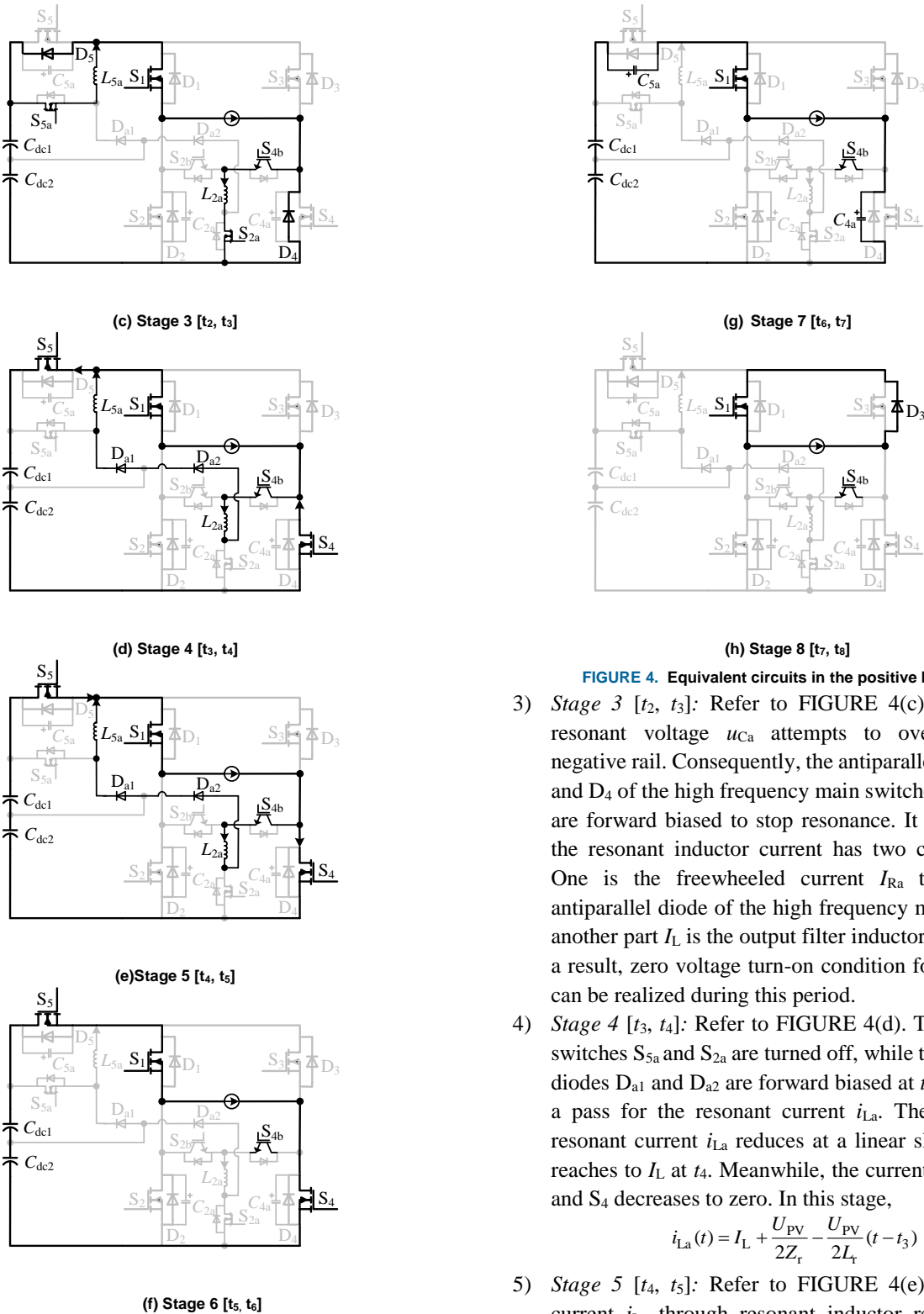**(g) Stage 7 [t_6, t_7]**

(h) Stage 8 [t_7, t_8]

FIGURE 4. Equivalent circuits in the positive half cycle

3) *Stage 3* [t_2, t_3]: Refer to FIGURE 4(c). At t_2, the resonant voltage u_{Ca} attempts to overshoot the negative rail. Consequently, the antiparallel diodes D_5 and D_4 of the high frequency main switches S_5 and S_4 are forward biased to stop resonance. It reveals that the resonant inductor current has two components. One is the freewheeled current I_{Ra} through the antiparallel diode of the high frequency main switch; another part I_L is the output filter inductor current. As a result, zero voltage turn-on condition for S_5 and S_4 can be realized during this period.

4) *Stage 4* [t_3, t_4]: Refer to FIGURE 4(d). The resonant switches S_{5a} and S_{2a} are turned off, while the auxiliary diodes D_{a1} and D_{a2} are forward biased at t_3 to provide a pass for the resonant current i_{La}. Thereafter, the resonant current i_{La} reduces at a linear slope until it reaches to I_L at t_4. Meanwhile, the current through S_5 and S_4 decreases to zero. In this stage,

$$i_{La}(t) = I_L + \frac{U_{PV}}{2Z_r} - \frac{U_{PV}}{2L_r}(t - t_3) \qquad (5)$$

5) *Stage 5* [t_4, t_5]: Refer to FIGURE 4(e). At t_4, the current i_{La} through resonant inductor reduces at a linear slope under the effect of the input voltage U_{PV} until it reaches to zero at t_5. Hence, auxiliary diodes D_{a1} and D_{a2} can be turned off with zero current, and their reverse recovery problem can be addressed. Meanwhile, the current through S_5 and S_4 is increased

linearly to I_L at t_5.

6) *Stage 6 [t_5, t_6]:* Refer to FIGURE 4(f). The ZVT-H5 comes into the normal power transmission stage again, which is same as the H5 topology.

7) *Stage 7 [t_6, t_7]:* Refer to FIGURE 4(g). At t_6, the high frequency main switches S_5 and S_4 are turned off. After that, capacitor voltages are charged at a linear slope under the effect of the filter inductor current I_L until the capacitor voltage increases to $0.5U_{PV}$ at t_7. As a result, the zero voltage turn-off condition for switches S_5 and S_4 can be realized. In this stage,

$$u_{Ca}(t) = \frac{I_L(t - t_6)}{C_r} \qquad (6)$$

8) *Stage 8 [t_7, t_8]:* Refer to FIGURE 4(h). The ZVT-H5 operation mode is the normal freewheeling stage. At t_8, the inverter goes back to *Stage 1* and starts a new switching cycle.

IV. RESONANT PARAMETER DESIGN AND CIRCUIT PERFORMANCE ANALYSIS

A. RESONANT PARAMETER DESIGN

The design steps of resonant parameters are described as follows.

1) The resonant inductor L_r and input DC voltage U_{PV} together decide the rising rate di/dt of the auxiliary switches within [t_0, t_1], which can be expressed as

$$\frac{di}{dt} = \frac{U_{PV}}{2L_r} \qquad (7)$$

The rising rate di/dt is normally less than 100 A/μs. Then, the value range of inductance can be calculated.

2) The resonant capacitor C_r is closely related to the zero-voltage turn-off process of high-frequency main switches, whose fall time t_f can be calculated as

$$t_f \leq \frac{U_{PV} \cdot C_r}{I_{Lp}} \qquad (8)$$

Where I_{Lp} represents the maximum on-state current. The value of C_r needs to be carefully chosen because a larger capacitance may increase peak current of the resonant tank, which results in more conduction losses, while a lower value of capacitance adds spike voltage across main switches.

3)The interval ($t_2 - t_1$) of resonance depends on both the inductance L_r and capacitance C_r. In order to maximize the effective duty cycle range realizing ZVT, the resonant interval should be as short as possible. The befitting resonant parameters should satisfy the following inequation

$$\frac{2I_{Lp}L_r}{U_{PV}} + \frac{\pi\sqrt{L_rC_r}}{2} \leq (5 \Box 15)\% \times T_s \qquad (9)$$

Firstly, the grid voltage of 220
V/50Hz and DC input voltage of 400 V are determined, and nominal parameters of ZVT-H5 prototype are chosen at 3 kW and 100 kHz. Subsequently, according to the

aforementioned steps, the resonant parameters L_r and C_r can be designed. The resonant inductance L_r is 5 μH under the condition of di/dt=40 A/μs, and the resonant capacitance C_r is chosen at 0.5 nF considering that the fall time t_f=8 ns for the MOSFET IPW65R041CFD. Finally, L_r=10 μH and C_r=5 nF are confirmed to meet the requirement (9).

B. VOLTAGE STRESSES ANALYSIS

As shown in FIGURE 3(c), voltage stresses of both high-frequency main switches (S_5 and S_2) and auxiliary switches (S_{5a} and S_{2a}) are equal half of the input voltage, which allows the employment of low-voltage-rated power devices in the high input voltage application. This can in turn decrease the auxiliary switches' turn-off switching loss and cost. Meanwhile, the voltage stress of resonant capacitors is also half of the input voltage because they are connected in parallel with corresponding main switches. This suggests that low-voltage-rated film capacitors can also be employed in ZVT-H5 to reduce the cost.

C. LOSS ANALYSIS OF POWER DEVICES

Analyzing power device losses is significant for the estimation of maximum efficiency of power electronic circuits. Power device losses of ZVT-H5 are evaluated to verify the enhanced efficiency compared with HS-H5.

1) SWITCHING LOSS

Based on the operation principle in Section III, the turn-on and turn-off losses of high-frequency main switches S_5, S_2 and S_4 are removed because ZVT conditions for these switches can be operated by the added resonant network, and the ZCS turn-on condition for high-frequency auxiliary switches S_{5a} and S_{2a} can be realized at the same time. The reduced turn-on and turn-off losses of main switches can be calculated as (10) and (11) [21], respectively.

$$W_{MOSFET,turn-on} = \frac{V_{DS}I_L(t_r + t_a + t_b)}{2} + \frac{V_{DS}I_{RM}t_b}{3} \qquad (10)$$

$$W_{MOSFET,turn-off} = \frac{V_{DS}I_Lt_{fr}^2}{2(t_{fr} + t_f)} + \frac{5V_{FR}I_Lt_{fr}^2}{6(t_{fr} + t_f)} \qquad (11)$$

where V_{DS} is the MOSFET's blocking voltage across the source and drain; I_L is the filter inductor current; I_{RM} is the reverse recovery current; V_{FR} is the diode forward peak voltage; and the rise time t_r, the fall time t_f, and diode reverse recovery time t_a, t_b are also included in the expressions.

Although undesired turn-off losses of S_{5a} and S_{2a} are included, there is still a decrease in the total switching losses in ZVT-H5, especially at high switching frequency.

2) CONDUCTION LOSS

According to FIGURE 3(c), the load current I_L gradually transfers from the freewheeling loop to the power process loop during the ZVT turn-on period [t_1, t_5] of main switches (S_5 and S_4). Moreover, the inverse process takes place during

This article has been accepted for publication in a future issue of this journal, but has not been fully edited. Content may change prior to final publication. Citation information: DOI
10.1109/ACCESS.2019.2946976, IEEE Access

IEEE *Access*

Author Name: Preparation of Papers for IEEE Access (February 2017)

the main switches' ZVT turn-off period [t_6, t_7]. Due to these operation modes, no extra current is superposed on the load current through main switches with added resonant action, which means that there is no obvious increase in conduction loss of main switches in power transmission process.

Meanwhile, FIGURE 4(h) reveals that the load current flows through S_1 and D_3 in the freewheeling period. The freewheeling loop of ZVT-H5 is the same as that of HS-H5, which results in equivalent conduction loss in the freewheeling period.

3) REVERSE RECOVERY LOSS

The reverse-recovery problem of the freewheeling diodes in HS-H5 can be addressed by the resonant inductors in ZVT-H5 in stage [t_4, t_5]. As a result, the reverse recovery related losses are removed, which also can enhance the conversion efficiency. The reduced reverse recovery related losses can be computed as

$$W_{\text{Diode,turn-off}} = \frac{V_{\text{F}}(I_{\text{L}} + I_{\text{RM}})(t_{\text{r}} + t_{\text{a}})}{2} + \frac{V_{\text{D}}I_{\text{RM}}t_{\text{b}}}{6} \qquad (12)$$

where V_{F} is the on-state voltage of the diode, and V_{D} is the diode's blocking voltage across the cathode and anode [21].

Additionally, considering that the added resonant tanks are activated in the transition period [t_0, t_3] of main switches, the loss of resonant components cannot be considered, which only accounts for about 13.5% of a switching cycle under the designed parameters.

Therefore, it can be concluded that the proposed topology ZVT-H5 has an advantage over HS-H5 in power device losses, especially at the increased switching frequency.

D. DIFFERENTIAL-MODE AND COMMON-MODE CHARACTERISTIC

Based on the operation mode analysis of ZVT-H5, differential-mode and common-mode voltages in all switching stages can be listed in TABLE I.

TABLE I
SWITCH STATES, DIFFERENTIAL-MODE, AND COMMON-MODE VOLTAGE OF THE ZVT-H5

Switching Stage	$u_{1\text{N}}$	$u_{2\text{N}}$	u_{DM}	u_{CM}
[t_0, t_1]	$U_{\text{PV}}/2$	$U_{\text{PV}}/2$	0	$U_{\text{PV}}/2$
[t_1, t_2]	$U_{\text{PV}} - u_{\text{C1a}}$	u_{C4a}	$U_{\text{PV}} - u_{\text{Ca}}$	$U_{\text{PV}}/2$
[t_2, t_6]	U_{PV}	0	U_{PV}	$U_{\text{PV}}/2$
[t_6, t_7]	$U_{\text{PV}} - u_{\text{C1a}}$	u_{C4a}	$U_{\text{PV}} - u_{\text{Ca}}$	$U_{\text{PV}}/2$
[t_7, t_8]	$U_{\text{PV}}/2$	$U_{\text{PV}}/2$	0	$U_{\text{PV}}/2$

As presented in the table, the differential-mode voltage u_{DM} of the ZVT-H5 is a unipolar SPWM style with low *dv/dt*, and the value of its common-mode voltage u_{CM} is equal to half of the input voltage in all switching stages. The constant common-mode performance enables the ZVT-H5 leakage current indicators to satisfy the grid standards, such as VDE0126-1-1, IEEE 1547 *et al*.

V. EXPERIMENTAL RESULTS AND DISCUSSIONS

In order to verify the effectiveness of main contributions in this study, a universal 3 kW ZVT-H5 prototype with the topology in FIGURE 3(a) and driving signal in FIGURE 3(b) have been developed and tested. Main involved components and their parameters are listed in Table Ⅱ. In Table Ⅱ, the resonant parameters L_{r}=10 μH and C_{r}=5 nF are selected and assembled. Two EI25 magnetic cores are employed as resonant inductors, whose winding is 12 turns. One 5 nF/ 800 V film capacitors is selected as the resonant capacitor to sustain the voltage rise when switches turn off. In this case, maximum value of grid-in current and resonant current I_{L}=19.28 A, I_{La}=22.05 A, switching period T_{r}=6.15μs, and the turn on current rise rate of main and auxiliary switches K=40 A/μs.

TABLE Ⅱ
PARAMETERS OF 3kW PROTOTYPE

Parameter	Value	
	ZVT-H5	HS-H5
Input voltage/V	360-400	
Grid voltage/V, frequency/Hz	180-240/50	
Rated power/W	3000	
Switching frequency/kHz	100	
DC-bus capacitor C_{dc1}, C_{dc2}/μF	3×470μF/350V	
Power device S_5, S_2, and S_4	IPW65R041CFD	
Power device S_1 and S_3	IKW40N60T	
Power device S_{5a}, S_{2a}	IPW65R041CFD	None
Power device S_{2b} and S_{4b}	IKW40N60T	None
Diode D_{a1}, D_{a2}	RHRG5060	None
Resonant inductors L_{1a}, L_{2a} /μH	10	None
Resonant capacitors $C_{1a}\sim C_{4a}$ /nF	5	None
Filter inductors L_1, L_2/ mH	0.5	
Filter capacitor C_1/μF	2	

FIGURE 5 (a) and (b) illustrates experimental waveforms of differential-mode and common-mode performances of the ZVT-H5 with rated parameters, respectively. FIGURE 5 (a) consists of the experimental waveforms of the grid voltage ug, grid-in current ig, and differential-mode voltage uDM at the grid frequency scale. The differential-mode voltage is a unipolar modulation style, which indicates that the inserted resonant tanks have no influence on the differential-mode performance of the ZVT-H5. Moreover, it is worth noting that the common-mode voltage u_{CM}=0.5*($u_{1\text{N}}+u_{2\text{N}}$) is a constant value during the whole grid period, and the common-mode performance of the ZVT-H5 is improved compared with that of the HS-H5 topology due to the clamping branch. Experimental results are in agreement with the theoretical analysis. In conclusion, the proposed ZVT-H5 has the unipolar SPWM differential-mode performance and constant common-mode performance, which is suitable for transformerless PV grid-connected applications.
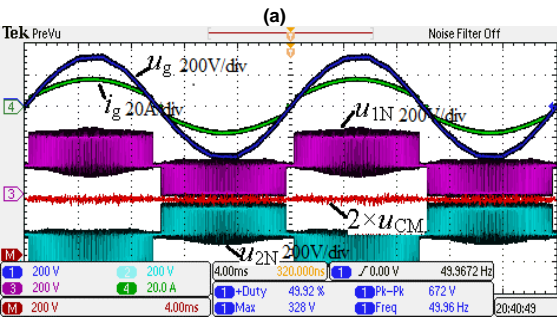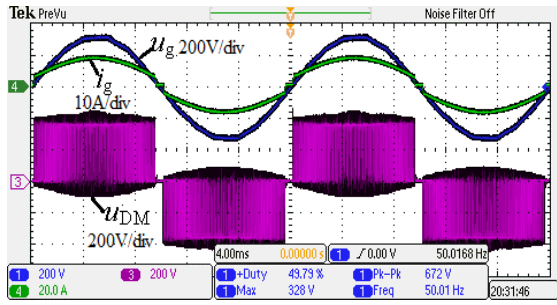
(a)

(b)

FIGURE 5. Experimental waveforms of the differential-mode voltage and common-mode voltage. (a) Differential-mode voltage at the grid frequency scale (u_g and u_{DM}: 200V/div, ig: 20A/div, and time: 4ms/div); (b) Common-mode voltage at the grid frequency scale (u_g, u_{1N}, u_{2N}, and u_{CM}: 200V/div, i_g: 20A/div, and time: 4ms/div).

FIGURE 6 presents waveforms of u_{GS5}, u_{GS5a}, the resonant voltage u_{C5a}, and the resonant current i_{L5a} of the resonant tank. Experimental waveforms of u_{GS5}, u_{GS5a}, the drain-source voltage u_{S5} and the passthrough current i_{S5} of the high-frequency main switch S_5 are shown in FIGURE 7. It is apparent that the antiparallel diode D_5 is already forward biased before S_5 turns on, which provides the zero-voltage turn-on condition for S_5. In addition, the voltage rising rate of S_5 is limited by the resonant capacitor C_{5a} during its turn-off period.

Experimental waveforms of u_{GS5}, u_{GS5a}, and the source current i_{S5a} and the drain-source voltage u_{DS5a} of the auxiliary switch S_{5a} are illustrated in FIGURE 8. It reveals that the rising rate of its turn-on current is limited by the resonant inductor L_{5a}. Therefore, the auxiliary switch S_{5a} can be turned on with zero current. The experimental waveforms of auxiliary diode D_{a1} are presented in FIGURE 9. When the auxiliary switches are turned off, the auxiliary diode is forward biased to provide the freewheeling path for the resonant current after the auxiliary switches are turned off. Aforementioned experimental waveforms are in agreement with the theoretical analysis in Section III.
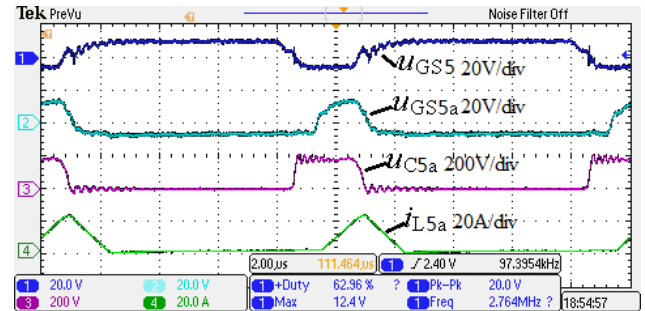

FIGURE 6. Experimental waveform of the resonant tank (u_{GS5} and u_{GS5a}: 25V/div, u_{C5a}: 200V/div, i_{L5a}: 20 A/div, and time: 2μs/div).
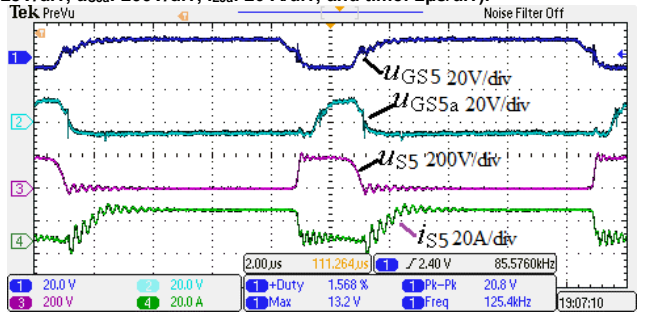

FIGURE 7. Experimental waveforms of the high frequency switch S_5 (u_{GS5} and u_{GS5a}: 25V/div, u_{S5}: 200V/div, i_{S5}: 20 A/div, and time: 2μs/div).

FIGURE 8. Experimental waveforms of the auxiliary switch S_{5a}. (u_{GS5} and u_{GS5a}: 25V/div, u_{S5a}: 200V/div, i_{S5a}: 20A/div, and time: 2μs/div).
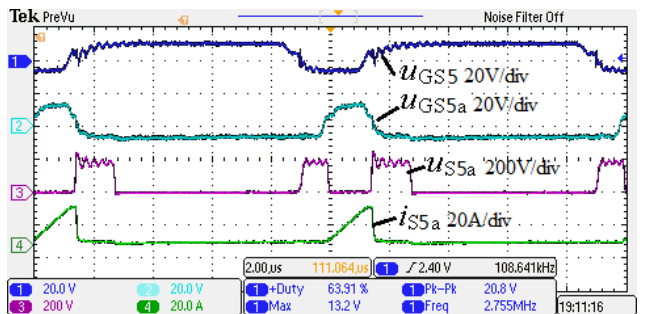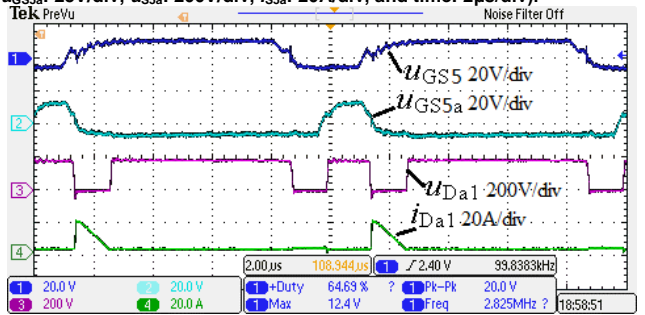

FIGURE 9. Experimental waveforms of the auxiliary diode D_{a1}. (u_{GS5} and u_{GS5a}: 25V/div, u_{Da1}: 200V/div, i_{Da1}: 20A/div, and time: 2μs/div).

TABLE III
PERFORMANCE COMPARISON AMONG TYPICAL HARD-SWITCHING TLI TOPOLOGIES AND THE PROPOSED ZVT-H5

		HERIC		H6-I		HS-H5		ZVT-H5	
Input DC capacitors	Quantity (piece)	1		2		1		2	
	Voltage	U_{PV}		$U_{PV}/2$		U_{PV}		$U_{PV}/2$	
	Price	High		Low		High		Low	
Switches	Quantity (piece)	4(HF[1])	2(LF[2])	2(HF)	4(LF)	3(HF)	2(LF)	5(HF)	4(LF)
	Voltage	U_{PV}	U_{PV}	$U_{PV}/2$	U_{PV}	U_{PV}	U_{PV}	$U_{PV}/2$	U_{PV}
	Price	High	Medium	Medium	Medium	High	Medium	Medium[3]	Medium
Diodes	Quantity (piece)	0		2		0		2	
	Voltage			$U_{PV}/2$				$U_{PV}/2$	
	Price	None		Low		None		Low	
Passive components	Quantity (set)	1(AC[4])		1(AC)		1(AC)		2(Aux[5])	
	Voltage/Current	U_{PV}/I_{Lp}[6]		U_{PV}/I_{Lp}		U_{PV}/I_{Lp}		$0.5U_{PV}/I_{Lp}+I_{La}$[7]	
	Price	High		High		High		Very low	
Losses	Switching	High		High		High		Low	
	Conduction	Low		High		Medium		Medium	
	Total	Medium		High		High		Low	
Heat-Sink (Volume/Price)		Medium		High		High		Medium	
EMI noise		High		High		High		Medium	
Leakage current		Medium		Medium		Medium		Low	

[1]: HF means high-frequency operation.

[2]: LF means line-frequency operation.

[3]: can choose low speed switches because of no switching losses.

[4]: AC means output filter at the AC side, which consists of inductor and capacitor.

[5]: Aux means resonant components in the resonant tank, which consists of inductor and capacitor.

[6]: I_{Lp} represents the maximum amplitude of the grid-in current.

[7]: I_{La} represents the maximum amplitude of the resonant current.

In order to verify the merit of the ZVT-H5 topology, efficiency curves of the ZVT-H5 and HS-H5 with 100 kHz switching frequency are shown in FIGURE 10. It suggests that the circulation loss of resonant tanks decreases the efficiency in a light load. However, with increasing the output power, the ZVT-H5 efficiency is improved compared with its hard-switching counterpart. This result indicates that increased resonant component losses are less than reduced switching losses in the ZVT-H5 topology.
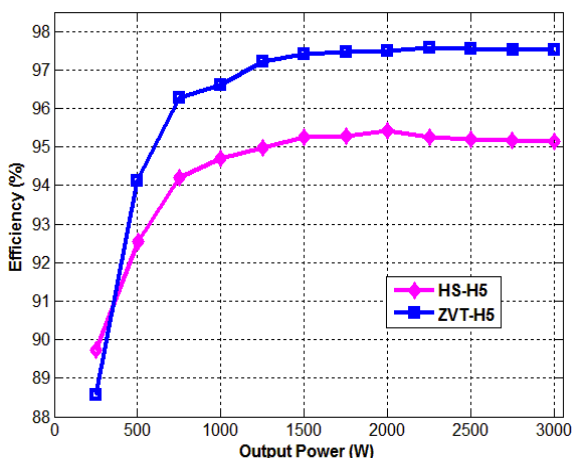

FIGURE 10. Efficiency curves comparison between the ZVT-H5 and HS-H5 (included the auxiliary power, such as drivers', controller's, and sensors', etc., and measured by Digital Power Analyzer VOLTECH PM3300).

Based on the above theoretical analysis and experimental data, the performance of the proposed ZVT-H5 topology and three typical hard-switching TLI topologies are summarized and compared in TABLE □. It can be concluded from the table that the major advantage of the ZVT-H5 is to reduce power device losses, which has been discussed in detail in section IV. This also can decrease the heat-sink volume as well as electro-magnetic interference (EMI) noise in turn. In addition, owing to the employment of clamping diodes, ZVT-H5 also gains an advantage in LC, which is one of the most important concerns for TLIs. However, as shown in the table, ZVT-H5 also has a disadvantage in terms of the number of passive components and diodes, which are essential for realizing ZVT. Fortunately, because the switching frequency of ZVT-H5 can be raised under the soft-switching operation, its ac filter can be shrunken to compensate for the increased cost of auxiliary resonant components and diodes.

VI. CONCLUSION

Simple and compact ZVT resonant tanks are proposed in this study. The presented ZVT-H5 inverter features the soft switching of the high-frequency main switches' turn-on and turn-off, the auxiliary switches' turn-on, and low voltage stresses across the auxiliary switches. In addition, the reverse-recovery problem of freewheeling diodes can be addressed by the resonant inductors to reduce the reverse recovery related losses. Moreover, the differential-mode feature of ZVT-H5 remains a unipolar modulation style. A

This article has been accepted for publication in a future issue of this journal, but has not been fully edited. Content may change prior to final publication. Citation information: DOI 10.1109/ACCESS.2019.2946976, IEEE Access

Author Name: Preparation of Papers for IEEE Access (February 2017)

3-kW prototype operating at 100 kHz is implemented and tested to verify the feasibility and merits of the proposed topology. In conclusion, ZVT-H5 topology has high efficiency and high power density, which can be regarded as potential candidate in the photovoltaic grid-connected system.

REFERENCES

REFERENCES

[1] L. Zhang, K. Sun, Y. Xing, and M. Xing, "H6 transformerless full-bridge PV grid-tied inverters," IEEE Trans. Power Electron., vol. 29, no. 3, pp. 1229–1238, Mar. 2014, doi: 10.1109/TPEL.2013.226017.

[2] Y. Gu, W. Li, Y. Zhao, B. Yang, C. Li, and X. He, "Transformerless inverter with virtual DC bus concept for cost-effective grid-connected PV power systems," IEEE Trans. Power Electron., vol. 28, no. 24, pp. 793–805, Feb. 2013, doi: 10.1109/TPEL.2012.2203612.

[3] B. Gu, J. Dominic, J.-S. Lai, C.-L. Chen, T. LaBella, and B. Chen, "High reliability and efficiency single-phase transformerless inverter for grid-connected photovoltaic systems," IEEE Trans. Power Electron., vol. 28, no. 5, pp. 2235–2245, May 2013, doi: 10.1109/TPEL.2012.2214237.

[4] H. Schmidt, C. Siedle, and J. Ketterer, "Wechselrichter zum umwandelneiner elektrischen gleichspannung in einen wechselstrom oder eine wechselspannung," EP Patent EP 1 369 985 A2, May 15, 2003.

[5] M. Victor, F. Greizer, S. Bremicker, and U. Hubler, "Method of converting a direct current voltage from a source of direct current voltage, more specifically from a photovoltaic source of direct current voltage, into an alternating current voltage," U.S. Patent US 20050286281 A1, Dec. 29, 2005.

[6] Islam M, Mekhilef S. H6-type transformerless single-phase inverter for grid-tied photovoltaic system[J]. Power Electronics Iet, 2015, 8(4):636-644.

[7] R. Gonzalez, E. Gubia, J. Lopez, and L. Marroyo, "Transformerless singlephase multilevel-based photovoltaic inverter," IEEE Trans. Ind. Electron., vol. 55, no. 7, pp. 2694–2702, Jul. 2008, doi: 10.1109/TIE.2008.924015

[8] Y. Xue, K. Divya, G. Griepentrog, M. Liviu, S. Suresh, and M. Manjrekar, " Towards next generation photovoltaic inverters," in Proc. IEEE Annu. IEEE Energy Convers. Congr. Expo., Sep. 2011, vol. 1, pp. 2467–2474, doi: 10.1109/ECCE.2011.6064096.

[9] B. Torsæter, S. Tiwari, R. Lund, and O.-M. Midtgard, "Experimental evaluation of switching characteristics, switching losses and snubber design for a full SiC half-bridge power module," in Proc. IEEE Int. Symp. Power Electron. Distrib. Gener. Syst., Jun. 2016, vol. 1, pp. 1–8, doi: 10.1109/PEDG.2016.7527071.

[10] Xia Y , Ayyanar R . "Inductor feedback ZVT based, low THD single phase full bridge inverter with hybrid modulation technique" IEEE APEC. 2017:3444-3450.

[11] D. Divan, "The resonant dc-link converter- a new concept in power conversion," IEEE Trans. Ind. Appl., vol. 25, no. 2, pp. 317–325, Mar./Apr.1989, doi: 10.1109/28.25548.

[12] H.-S. Choi, Y. Cho, J. Kim, and B. Cho, "Grid-connected photovoltaic inverter with zero-current switching," in Proc. Int. Conf. Power Electron., 2001, pp. 251–255.

[13] Y.-H. Kim, J.-G. Kim, Y.-H. Ji, C.-Y. Won, and Y.-C. Jung, "Photovoltaic parallel resonant DC-link soft switching inverter using hysteresis current control," in Proc. IEEE Appl. Power Electron. Conf., vol. 3, Feb. 2010, pp. 2275–2280, doi: 10.1109/APEC.2010.5433553.

[14] M. Amirabadi, A. Balakrishnan, H. A. Toliyat, and W. C. Alexander, "High-frequency AC-link PV inverter," IEEE Trans. Ind. Electron., vol. 61, no. 1, pp. 281–291, Jan. 2014, doi: 10.1109/TIE.2013.2245616.

[15] M. W. Gekeler, "Soft switching three level inverter with passive snubber circuit (S3L inverter)," in Proc. Eur. Conf. Power Electron. Appl., vol. 1, Sep. 2011, pp. 1–10.

[16] S. V. Araujo, P. Zacharias, R. Mallwitz (2010) Highly efficient single-phase transformerless inverters for grid-connected photovoltaic systems. IEEE Trans. Industrial Electronics 57(9): 3118~ 3128.

[17] Xiao HF, Liu XP, and Lan K (2014) Zero-voltage-transition full bridge topologies for transformerless photovoltaic grid-connected inverter. IEEE Trans. Industrial Electronics 61(10): 5393~5401.

[18] Xiao HF, Xie SJ, Yang C, and Huang RH (2011) An optimized transformerless photovoltaic grid-connected inverter. IEEE Trans. Ind. Electron. 58(5): 1887-1895

[19] L. Zhang, K. Sun, L. Feng, H. Wu, Y. Xing, "A Family of Neutral Point Clamped Full-Bridge Topologies for Transformerless Photovoltaic Grid-Tied Inverters," IEEE Trans. Power Electron., vol. 28, no. 2, pp. 730–739, Feb. 2013, doi: 10.1109/TPEL.2012.2205406.

[20] Li W. Gu Y. Luo H. et al. "Topology review and derivation methodology of single-phase transformerless photovoltaic inverters for leakage current suppression," IEEE Trans. on Industrial Electronics. vol. 62, no.7, pp. 4537–4551, Jul. 2015, doi: 10.1109/TIE.2015.2399278.

[21] F. Hong, R. Z. Shan, H. Z. Wang, and Y. Yangon, "Analysis and calculation of inverter power loss," Proc. CSEE, vol. 28, no. 15, pp. 72–78, May 2008.

JICHENG FANG was born in Nanjing, Jiangsu Province, China, in 1995. He received the B.S. degrees in electrical engineering from the Nanjing Institute of Technology, Nanjing，China, from 2013 to 2017, and he is currently working toward the M.S. degree in electrical engineering with Shanghai University of Electric Power, Shanghai, China, from 2017. His current research interests include hybrid energy storage，smart grid, and micro grid energy management.

MINGMING SHI was born in Nanjing, Jiangsu Province, China, in 1986. He received the B.S. and Ph.D. degrees in electrical engineering from the Nanjing University of Aeronautics and Astronautics (NUAA), in 2007 and 2012, respectively. Since 2012, he joined in State Grid Jiangsu Electric Power Co., LTD. Research Institute (JSEPRI). Now he is the deputy director of New energy & Distribution Grid department. His research is focusing on DC distributed generation systems, power quality analysis, Renewable Energy and Microgrid.

HUAFENG XIAO (S'10–M'13–SM'17) was born in Hubei, China. He received the B.S., M. S., and Ph.D. degrees in electrical engineering from Nanjing University of Aeronautics and Astronautics, Nanjing, China, in 2004, 2007, and 2010, respectively. He joined the Faculty of Power Electronics in 2011, and is currently an Associate Professor with the College of Electrical Engineering, Southeast University, Nanjing, China. From 2015 to 2016, he was a Postdoctoral Fellow with the Department of Electrical and Computer Engineering, Ryerson University, Toronto, ON, Canada. From August 2016 to 2017, he was a Postdoctoral Fellow with the Department of Electrical and Computer

IEEE *Access*

Engineering, McGill University, Montreal, QC, Canada. He has authored more than 50 technical papers in journals and conference proceedings, and held 16 China patents. His research interests include high-frequency soft-switching conversions, photovoltaic power systems, and applications of power electronic technology in power systems.

RUIBIN WANG was born in Changzhou, Jiangsu Province, China, in 1996. He received the B.S. degree in electrical engineering from Hebei University of Technology, Tianjin, China, in 2018, and is currently working toward the M.S. degree in electrical engineering at Southeast University, Nanjing, China. His current research interests include high-frequency soft-switching conversion and photovoltaic applications.